Influences of deformation parameters on wobbling motion

H. M. Dai and Q. B. Chen*
Department of Physics, East China Normal University, Shanghai 200241, China

(Received 6 February 2024; revised 17 April 2024; accepted 9 May 2024; published 23 May 2024)

The influences of deformation parameters β and γ on the wobbling motion have been investigated in the framework of particle rotor model taking the valence nucleon $h_{11/2}$ and $i_{13/2}$ combined with a triaxial core as examples. Comprehensive examinations have been carried out to assess the influence of β and γ on the wobbling frequencies, electromagnetic transition probabilities, and angular momentum geometries. It is demonstrated that larger β and smaller γ favors the formation of transverse wobbling. In addition, a smaller β leads to a smaller transverse wobbling energy, while a larger longitudinal wobbling energy. These behaviors can be well explained by the harmonic frozen alignment approximation method.

DOI: 10.1103/PhysRevC.109.054321

I. INTRODUCTION

Wobbling motion was first predicted for a nucleus with stable triaxial deformation by Bohr and Mottelson in the 1970s [1]. Due to unequal moments of inertia, rotation around nonpreferred axes causes deviation from the principal axis, resulting in wobbling motion.

When the triaxial rotor is coupled with a high-j valence particle, two distinct wobbling modes were identified by Frauendorf and Dönau: longitudinal wobbling (LW) and transverse wobbling (TW) [2]. In the LW (TW), the angular momentum of the high-j valence particles is parallel (perpendicular) to the principal axis with the largest moment of inertia. Both LW and TW exhibit enhanced $I \to I-1$ $E2$ transitions between adjacent wobbling bands, characterized by a series of $E2$ rotational bands corresponding to the different wobbling quanta. The variation trend of the excitation energy of wobbling motion, called wobbling frequency or wobbling energy, is used to distinguish different types of wobbling modes. The wobbling frequency of a LW increases with spin, while that of a TW decreases [2]. Later on, Chen and Frauendorf further proposed a comprehensive classification based on the topology of the classical orbits that are visualized using the spin coherent state (SCS) maps [3]. Explicitly, the LW corresponds to a revolution of total angular momentum $\boldsymbol{J}$ around the axis with the largest moment of inertia and TW a revolution of $\boldsymbol{J}$ around an axis perpendicular to the axis with the largest moment of inertia.

Experimentally, the phenomenon of wobbling was first discovered in 2001 [4]. The ^{163}Lu is the first discovered wobbling nucleus for the one-phonon wobbling excitation [4] in 2001 and in 2002 for the two-phonon wobbling excitation [5], which was later interpreted as TW [2]. After that, the wobbling nuclei in the $A \approx 160$ mass region were reported, including ^{161}Lu [6], ^{165}Lu [7], ^{167}Lu [8], ^{167}Ta [9], and the latest ^{151}Eu [10]. After the concept of LW and TW was proposed, the wobbling motion in other mass regions was also well explored. In detail, in the $A \approx 130$ mass region, there are candidates ^{135}Pr [11,12], ^{133}La [13], ^{130}Ba [14–16], ^{127}Xe [17], ^{133}Ba [18], and ^{136}Nd [19,20]. In the heavier $A \approx 190$ mass region, two candidates ^{187}Au [21] and ^{183}Au [22] were reported. In the lighter $A \approx 100$ mass region, there is only one experimental candidate ^{105}Pd [23] and several predicted candidates in the isotones of ^{105}Pd [24]. Moreover, in the $A \approx 60$ mass region, wobbling candidates were also predicted in the Ni isotopes [25]. It is worth pointing out that the wobbling motion can exist in the nucleus with deformation ranging from small to large. For example, the wobbling nuclei reported in the $A \approx 160$ mass region are built on the $i_{13/2}$ configuration with significantly large deformations ($\beta \approx 0.40$), while in the other mass regions on the $h_{11/2}$ configuration with small deformation ($\beta \approx 0.20$).

Since the concept of wobbling motion [1] was put forward, many theoretical models have been developed, such as the random-phase approximation (RPA) method [26–37], the collective Hamiltonian method [38–40], and the angular momentum projection method [12,16,19,41]. Here, it is worth emphasizing that the RPA study started right after Bohr and Mottelson's prediction [1], aiming at microscopically justifying the triaxial rotor model [26]. More RPA work preceding the experimental discovery [4] can be refereed to the references cited in Ref. [27]. Furthermore, the triaxial particle-rotor model (PRM) serves as the main framework for describing various physical quantities associated with the wobbling motion [2,3,15,21–24,42–48]. Additionally, some approximate methods for solving the PRM have also been utilized to study wobbling motion [49–53]. The PRM provides a systematic and quantitative approach to analyze and understand wobbling motion by considering the coupling between the rotational degrees of freedom of the core and the motion of the valence particles. Through the PRM, energy spectra, electromagnetic transitions, and other observable related to wobbling motion can be obtained, which is highly suitable for the systematic study of wobbling motion due to its advantages of providing a simple solution and requiring less computational effort.

The phenomenon of wobbling motion in atomic nuclei serves as a pivotal criterion for assessing the presence of

*Corresponding author: qbchen@phy.ecnu.edu.cn

triaxial deformation. The existence of wobbling motion in an odd-mass nucleus is contingent upon the satisfaction of two critical prerequisites: first, the existence of a high-j particle or hole, and second, the manifestation of pronounced triaxial deformation γ [1–3]. Extensive theoretical investigations have elucidated that the intrinsic properties of the high-j particle or hole plays a decisive role in characterizing the nature and dynamics of the wobbling motion [2,3,48]. Moreover, deformation parameters, representing the second essential condition for the emergence of wobbling motion, warrant thorough investigation. Observational evidence and theoretical analyses has delineated a marked distinction in the stability and persistence of TW across different mass regions and deformation regimes. Specifically, in the context of strongly deformed nuclei within the mass region $A \approx 160$, TW exhibits enhanced stability and extends over a broader range of spin compared to its manifestation in nuclei characterized by lower deformation in alternative mass regions [2,3]. This observation prompts a deeper inquiry into the underlying mechanisms governing the stability of wobbling motion with a particular emphasis on the role of nuclear deformation parameters.

In this paper, we aim to comprehensively analyze the impact of quadrupole deformation parameters, specifically β and γ, on the wobbling frequencies, electromagnetic transition probabilities, as well as angular momentum geometries in the framework of PRM. Our investigation focuses on the system with valence nucleons $h_{11/2}$ and $i_{13/2}$ in combination with a triaxial core. A focal point is to elucidate the mechanism underlying the observed phenomenon where TW exhibits markedly greater stability in nuclei with strong deformation compared to those with lower deformation. Through this study, we aim to shed light on the intricate interplay between nuclear deformation parameters and the dynamical properties of wobbling motion.

II. NUMERICAL DETAILS

We consider the systems consisting of a triaxial rotor and a single proton particle locating at $h_{11/2}$ or $i_{13/2}$ shells. The triaxial deformation parameter is taken as $\gamma = 20^\circ$, 30°, and 40° and the quadrupole deformation parameter β for the single-particle Hamiltonian is taken as 0.1, 0.2, 0.3, 0.4, and 0.5. The moment of inertia for the triaxial rotor is adopted as irrotational flow type $\mathcal{J}_k = \mathcal{J}_0 \sin^2(\gamma - 2k\pi/3)$ with $\mathcal{J}_0 = 20\,\hbar^2/\text{MeV}$. The ratios between the three moments of inertia for the intermediate (m), short (s), and long (l) axis is $\mathcal{J}_m/\mathcal{J}_s/\mathcal{J}_l \approx 1.00/0.43/0.12$ for $\gamma = 20^\circ$, $\mathcal{J}_m/\mathcal{J}_s/\mathcal{J}_l = 1.00/0.25/0.25$ for $\gamma = 30^\circ$, and $\mathcal{J}_m/\mathcal{J}_s/\mathcal{J}_l \approx 1.00/0.12/0.43$ for $\gamma = 40^\circ$. For the electromagnetic transition probabilities, the intrinsic charge quadrupole momentum $Q_0 = (3/\sqrt{5\pi})R_0^2 Z\beta$ and the g factors $g_p - g_R$ are 0.80 for $h_{11/2}$ and 0.74 for $i_{13/2}$.

III. RESULTS AND DISCUSSION

A. Energy spectra and electromagnetic properties

Based on the PRM, the variation of energy differences as well as the electromagnetic transition probability ratios for the $h_{11/2}$ and $i_{13/2}$ configurations with different deformation parameters are shown in Fig. 1. The energy difference between the obtained bands B2 ($n = 1$) and B1 ($n = 0$) is calculated as

$$\Delta E(I) = E_{\text{B2}}(I) - [E_{\text{B1}}(I+1) + E_{\text{B1}}(I-1)]/2. \quad (1)$$

As aforementioned, the change in ΔE can reflect the type of wobbling motion. The decreasing ΔE is a hint of TW, while the increasing one corresponds to a LW [2,3]. For $h_{11/2}$ with $\gamma = 20^\circ$, ΔE shows a trend of first decreasing and then increasing. This indicates that it is a TW in the low spin region and a LW in the high spin region, consistent with the previous work [2,3,48]. The magnitude of ΔE varies with deformation β. When β is small, e.g., $\beta = 0.1$, the ΔE change is very small in the low spin region, showing less pronounced TW characteristics. Moreover, the minimum value of ΔE appears at $I = 10.5\hbar$, followed by LW. A smaller β corresponds to a smaller ΔE at low spin. For the fixed γ, e.g., $\gamma = 20^\circ$, with the increase of β, the nucleus is more likely to exhibit TW in the low spin region. In addition, the positions of the turning points of ΔE for different β are different. For example, for $\beta = 0.2$ and 0.3, it occurs at $I = 12.5\hbar$, while for $\beta = 0.4$ and 0.5 at $I = 14.5\hbar$. One notes that these TW spin regions are much shorter than those observed in Lu isotopes, reaching up to $40\hbar$ [54]. The reason is attributed to that the ratio $\mathcal{J}_s/\mathcal{J}_m$ used in the calculation ($\approx$0.12, 0.25, and 0.43) is much smaller than the realistic cases ($\approx$0.85 [2]). With the increase of spin, the magnitude of ΔE for larger β becomes smaller, exhibiting distinct behaviors with the cases of low spin region.

Different from the ΔE at $\gamma = 20^\circ$, all ΔE at $\gamma = 30^\circ$ within the low spin region, including $\beta = 0.1$, shows a significant decrease. Moreover, the turning point of transition from TW to LW shifts towards to the lower spin region. By focusing on the wobbling bands with large β, one notes that the ΔE increases slowly in the high spin region. The characteristics of LW become less distinct. As γ increases to 40°, the TW of the $h_{11/2}$ configuration disappears. The nucleus with $\beta = 0.1$ exhibits LW throughout the entire spin region, and as β increases, LW gradually disappears, indicating the absence of wobbling motion. Specifically, $\Delta E < 0$ happens at some spins, which means that the wobbling excitation is unstable. Similar characteristics are observed in the wobbling energy of the $i_{13/2}$ configuration. In short, within the studied range of deformations, TW is more likely to form at larger β and smaller γ. Compared to triaxial deformation γ, LW shows higher sensitivity to β.

The investigation of electromagnetic transition probabilities plays a crucial role in experimental studies focused on wobbling motion. An experimental hallmark of wobbling on the electromagnetic transition probability is the collective enhancement of $I \to I-1$ $B(E2)$ values for transitions from the excited band to the yrast band [2,3]. This enhancement arises due to the collective motion of the charged system, which differs from the scenario observed in the traditional signature partner bands. To check the electromagnetic properties of the discussed systems, we further illustrate the variations of $B(E2)_{\text{out}}/B(E2)_{\text{in}}$ and $B(M1)_{\text{out}}/B(E2)_{\text{in}}$ for the $h_{11/2}$ and $i_{13/2}$ configurations with different deformation parameters in

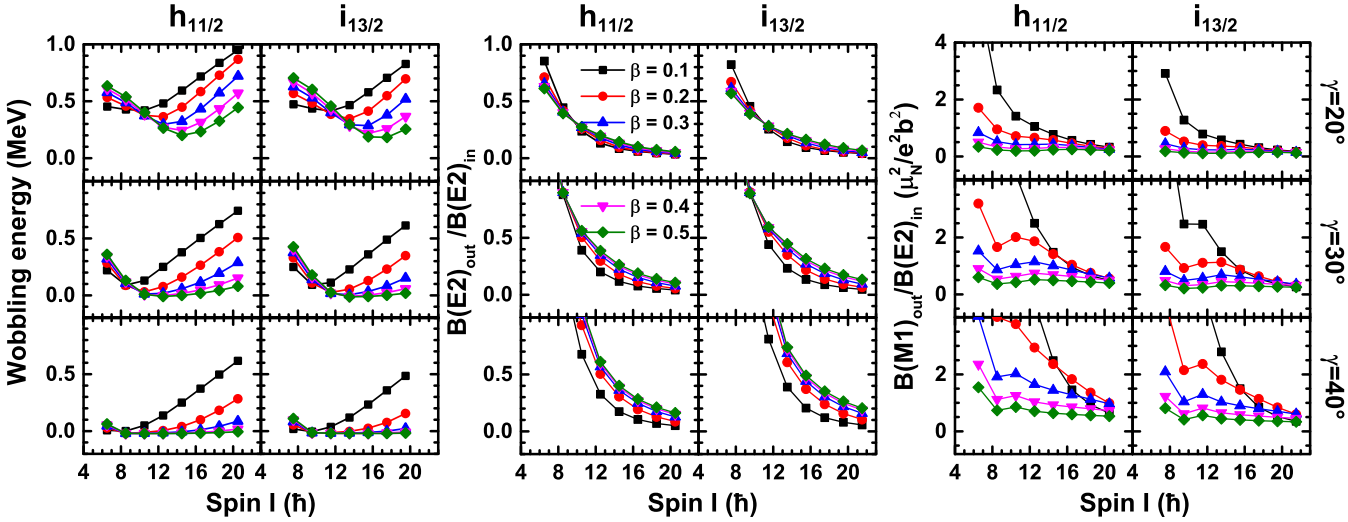

FIG. 1. The calculated wobbling energies (left panels) as well as the electromagnetic transition probability ratios $B(E2)_{\rm out}/B(E2)_{\rm in}$ (middle panels) and $B(M1)_{\rm out}/B(E2)_{\rm in}$ (right panels) as functions of spin I by the PRM for the $h_{11/2}$ and $i_{13/2}$ configurations with different deformation parameters β and γ. Here, the suffices "in" and "out" refer to the intraband $\Delta I = 2$ and interband $\Delta I = 1$ transitions that connect the bands, respectively.

Fig. 1. Here, the suffices "in" and "out" refer to the intraband $\Delta I = 2$ and interband $\Delta I = 1$ transitions that connect the bands, respectively. Under the same γ, the variation of the $B(E2)_{\rm out}/B(E2)_{\rm in}$ ratio for $h_{11/2}$ and $i_{13/2}$ is not significant across different β values. The difference of $B(E2)_{\rm out}/B(E2)_{\rm in}$ mainly comes from γ deformation. Additionally, there is a significant variation in $B(E2)_{\rm out}/B(E2)_{\rm in}$ in the low spin region.

Compared to $B(E2)_{\rm out}/B(E2)_{\rm in}$, the variation rate of $B(M1)_{\rm out}/B(E2)_{\rm in}$ is more sensitive to the β. The value of $B(M1)_{\rm out}/B(E2)_{\rm in}$ for small β is larger than that for large β, which is attributed to the fact that the intrinsic quadrupole momentum Q_0 is proportion to β and results in $B(E2)_{\rm in}$ value proportion to β^2. Additionally, the ratio of $B(M1)_{\rm out}/B(E2)_{\rm in}$ increases with an increase in triaxial deformation γ.

Furthermore, it is important to note that the behavior of $B(M1)_{\rm out}/B(E2)_{\rm in}$ for $\gamma = 30^\circ$ and 40° exhibits nonsmooth characteristics at specific spin values. It is revealed that this nonsmooth behavior stems from the dynamics of $B(M1)_{\rm out}$. In Fig. 2, we present the calculated $B(M1)_{\rm out}$ as functions of spin I by the PRM for the $h_{11/2}$ configuration with different deformation parameters β and γ. We find that the nonsmooth behavior of $B(M1)_{\rm out}$ correlation with the critical spin value marking the transition from TW to LW. This observation suggests that the nonsmooth behavior arises from single-particle motion. Interestingly, we observed that compared to small γ, the nonsmooth behavior in $B(M1)_{\rm out}$ is more pronounced for large γ. This can be attributed to, as we will show in the following, the enhanced ease with which valence nucleons are transferred from the s axis to the m axis when γ is large. This insight highlights that the nonsmooth behavior of $B(M1)_{\rm out}/B(E2)_{\rm in}$ or $B(M1)_{\rm out}$ can serve as a criterion for distinguishing the wobbling mode. Specifically, the nonsmooth features in the behavior of $B(M1)_{\rm out}/B(E2)_{\rm in}$ or $B(M1)_{\rm out}$ can provide valuable indicators for identifying the transition from TW to LW within the nucleus.

B. Distinguish wobbling modes

To begin with, the judgment of the wobbling motion type is based on varying deformation parameters. The total angular momentum serves as an effective tool for intuitively exploring the types of wobbling motion for understanding the

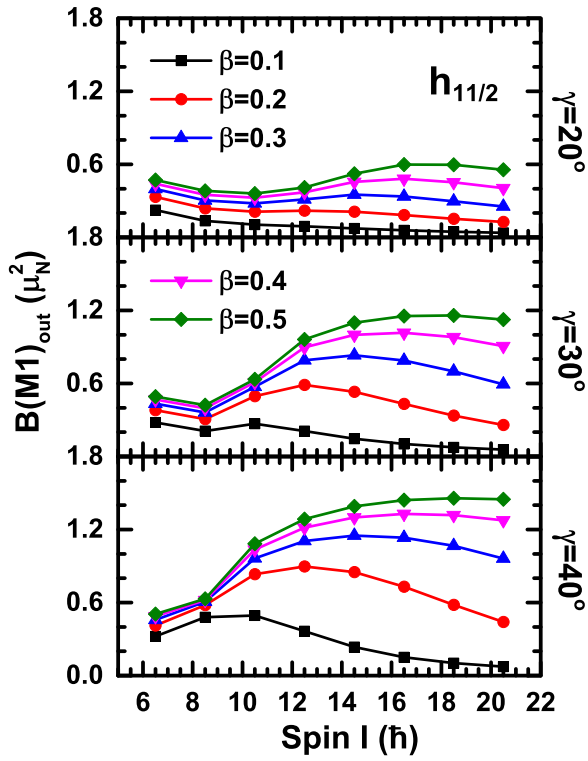

FIG. 2. The calculated $B(M1)_{\rm out}$ as functions of spin I by the PRM with different deformation parameters β and γ for the $h_{11/2}$ configuration.

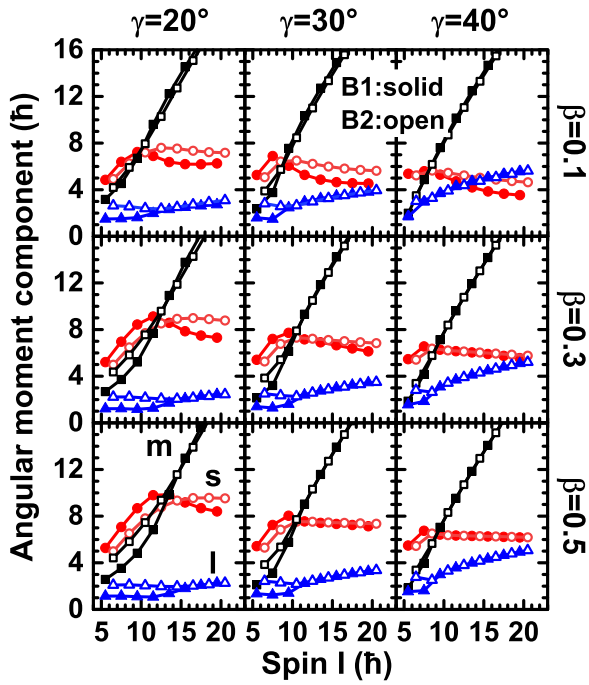

FIG. 3. Total angular momentum components along the intermediate (m), short (s), and long (l) axes for the lowest bands B1 and B2 calculated by PRM with different deformation parameters β and γ for the $h_{11/2}$ configuration.

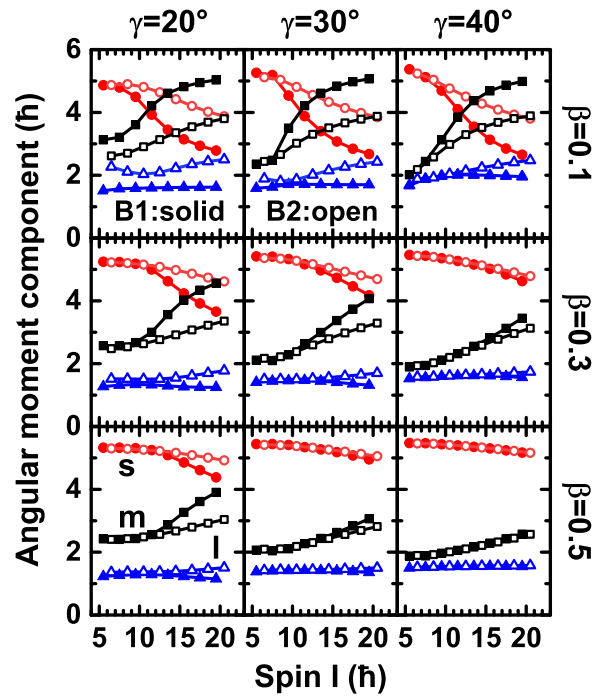

FIG. 4. Same as Fig. 3, but for the particle angular momentum.

underlying physics [3]. Taking the $h_{11/2}$ configuration case as an example, the components of the total angular momentum on the three principal axes for the calculated bands B1 and B2 with different deformation parameters are shown in Fig. 3. In the low spin region, the total angular momentum component along the s axis is the largest, followed by the m axis, and the l axis is the smallest. This reflects that the angular momentum of the nucleus is mainly aligned along the s axis. This is the picture of TW [3], consistent with the phenomenon presented in Fig. 1.

As spin increases, the s component of the total angular momentum increases and tends to stabilize at a certain spin. The m component continuously increases and eventually dominates. In contrast, the change of l component is relatively small. This indicates that the competitions between the s and m components are different under different deformation parameters. For $\beta = 0.1$ and $\gamma = 20^\circ$, the s component is larger than the m one when $I < 8.5\hbar$, consistent with the results in Fig. 1, indicating TW in the low spin region. With the same γ, a larger value of β corresponds to a higher critical spin for TW.

C. Role of single particle

In order to further explore the influence of deformation parameters on the wobbling motion, Fig. 4 shows how the particle angular momentum components change with spin for $h_{11/2}$ configuration with different deformation parameters. For $\beta = 0.1$ and $\gamma = 20^\circ$, the s component is about $5\hbar$ at the beginning, higher than those of m and l components. When $I > 8\hbar$, the s component begins to decrease rapidly, and the m component begins to increase. This behavior is generated because the core and valence nucleons produce a strong Coriolis force and the core tries to drive the particles to align along the m axis, making the energy lower. As spin increases, the m component increases and eventually exceeds the s one. This also implies that as the spin increases, the wobbling mode changes from TW to LW, consistent with the phenomenon observed in Fig. 1. In addition, the l component does not change much in the whole spin region.

Next, let us examine the influence of the parameter β on the particle angular momentum while keeping the triaxial deformation γ. In this analysis, we focus on the example of a $h_{11/2}$ nucleon with $\gamma = 20^\circ$. Upon investigating different values of β, it becomes evident that the angular momentum of the l axis remains relatively unchanged. The significant changes in angular momentum occur primarily in the s and m components. Moreover, in the whole spin region, the s and m components change more rapidly for smaller β, and the change rate of band B1 is larger than that of band B2. Corresponding to Fig. 1, the wobbling energy of the larger β can maintain the TW to a larger spin region.

For the same β, the larger γ corresponds to the larger s component and smaller m component at the beginning of rotation. The change in the l component remains insignificant throughout the entire spin region. Within the studied spin region, the angular momentum in the s axis decreases while the angular momentum in the m axis increases.

Furthermore, one notes that there are differences in the variations of bands B1 and B2. With an increase in γ, the decrease in the s component of band B1 becomes weaker, and the corresponding increase in the m component of band B1 becomes slower. On the other hand, the decrease in the s component of band B2 is more pronounced at large γ

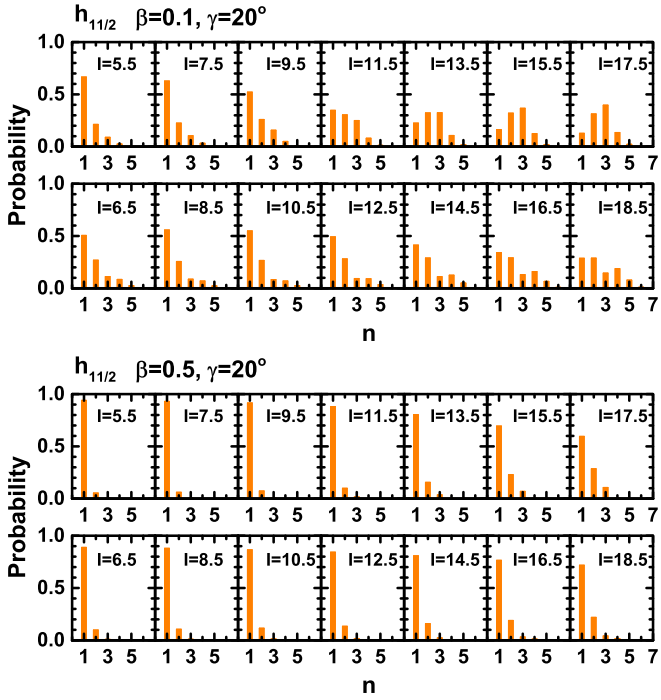

FIG. 5. Probability distributions and for the single-particle state (n-plot P_n) calculated by the PRM for states in the bands B1 (with $I = 2m - 1/2$) and B2 (with $I = 2m + 1/2$) of $h_{11/2}$ configuration with $\gamma = 20^\circ$ for $\beta = 0.1$ (upper panels) and 0.5 (lower panels). The numbers $n = 1, 2,..., 6$ correspond to the single-particle states with third angular momentum components k approximating to $\pm 1/2$, $\pm 3/2,..., \pm 11/2$.

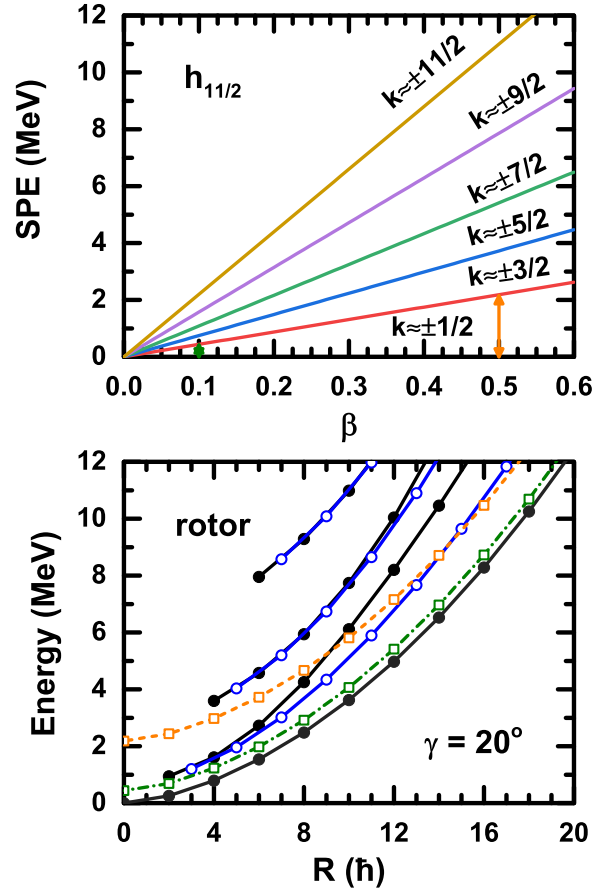

FIG. 6. Upper panel: The triaxial $h_{11/2}$ shell ($\gamma = 20^\circ$) single-particle energies ε_n with respect to the lowest energy level as a function of β. The corresponding third angular momentum components k are $\pm 1/2$, $\pm 3/2,...,$ $\pm 11/2$ at $\gamma = 20^\circ$ (which is a good quantum number only for $\beta = 0^\circ$). The arrows between the $k \approx \pm 1/2$ and $\pm 3/2$ levels indicate the energy spacing for the two levels at small deformation $\beta = 0.1$ and large deformation $\beta = 0.5$. Lower panel: Triaxial rotor energies ($\gamma = 20^\circ$) as functions of its angular momentum R. The full dots with solid lines belong to the states with signature $\alpha = 0$, while the empty dots with solid lines to signature $\alpha = 1$. The empty dots with dashed lines are obtained by shifting the lowest energy with a value of the energy splitting between the $k \approx \pm 1/2$ and $\pm 3/2$ levels at $\beta = 0.1$ (dot-dashed line) and $\beta = 0.5$ (dashed line).

compared to small γ, and the increase in the m component is more prominent at larger deformations. These observations indicate a competitive relationship between the changes in bands B1 and B2.

Considering the importance of valence nucleons in wobbling motion under different deformation parameters β, probability distributions for the single-particle state (n-plot P_n) calculated in the PRM for bands B1 and B2 of the $h_{11/2}$ configuration with $\gamma = 20^\circ$ for $\beta = 0.1$ and 0.5 are presented in Fig. 5. The index n is in accordance with the increasing energy of the single-particle state. For the $h_{11/2}$ configuration, there are six double-fold degenerated energy levels, i.e., $n = 1, 2,..., 6$. For $\beta = 0.1$, the angular momentum is mainly composed of $n = 1$ at $I = 5.5\hbar$. As spin increases, the angular momentum distribution of the valence nucleon becomes more and more mixed. Different from $\beta = 0.1$, the angular momentum distribution in $\beta = 0.5$ mixing is less. This results in a less change in the angular momentum of the nuclear with larger β.

In the following, we will further explore why the nucleus with smaller γ and larger β are more prone to undergo TW. The γ directly affects the value of the moment of inertia. When the triaxial deformation parameter γ is smaller, the ratio $\mathcal{J}_s/\mathcal{J}_m$ becomes larger. This results in that the angular momentum is more aligned towards the s axis, making it easier to form TW.

How does the quadrupole deformation parameter β affect the wobbling motion? To answer this question, we show in Fig. 6 the single-particle energies ε_n of the $h_{11/2}$ shell ($\gamma = 20^\circ$) relative to the lowest energy level as a function of β, and the energies of the triaxial rotor ($\gamma = 20^\circ$) as functions of its angular momentum R. The single-particle energy levels exhibit a linear variation with increasing β. The arrows between the $k \approx \pm 1/2$ ($n = 1$ level) and $\pm 3/2$ ($n = 2$ level) levels represent the energy splitting between these two levels for small deformation ($\beta = 0.1$) and large deformation ($\beta = 0.5$). The energy splitting at $\beta = 0.5$ is significantly larger than that at $\beta = 0.1$. Shifting the energy difference between the $k \approx \pm 1/2$ and $\pm 3/2$ levels at $\beta = 0.1$ and $\beta = 0.5$ to the core R ground state energy yields the dot-dashed line and

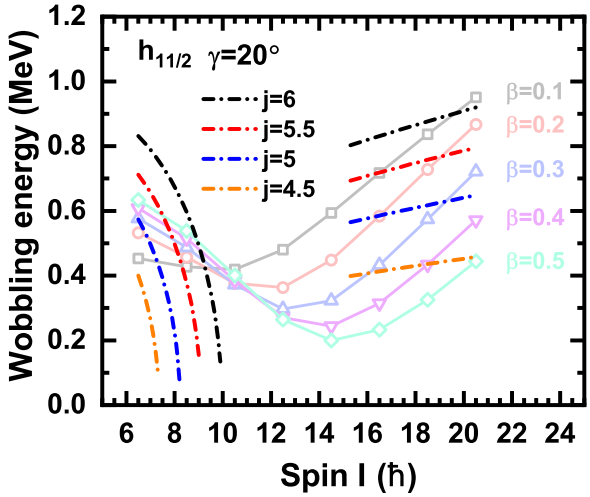

FIG. 7. The calculated wobbling energies as functions of spin I by the HFA (lines) in comparison with those by the PRM (line with symbols) for the $h_{11/2}$ with $\gamma = 20°$. For the HFA results, we fix j on the s axis (low spin) and m axis (high spin) and calculate the wobbling energy using Eq. (2).

dashed line in the lower panel of Fig. 6. Clearly, under the same γ, a higher rotor angular momentum and rotor excitation energy are required to have comparable excitation with the valence nucleon excitation energy from $k \approx \pm 1/2$ to $\pm 3/2$ for $\beta = 0.5$ than that for $\beta = 0.1$. This explains the much less mixed in the n-plot P_n of Fig. 6 and the characteristic of TW exhibiting wobbling energy over a wider range in Fig. 1 for the larger β.

D. Harmonic frozen alignment analysis

In Ref. [2], the harmonic frozen alignment (HFA) approximation method was proposed to analysis the rotational properties of TW and LW. Preceding Ref. [2], the method essentially the same as the HFA approximation has been utilized in Ref. [32] to give an explanation of the calculated dependence of the wobbling energy on the rotational frequency in the ^{163}Lu, i.e., increasing in the lower frequency and decreasing in the higher frequency (can also c.f. right panel of Fig. 8). The advantage of HFA method is that it can describe the wobbling frequency and transition probability in a simple analytical expressions, thus providing a qualitative understanding of the wobbling motion. In the following, we will also use the HFA to understand the behavior of the wobbling energy with respect to the deformation parameters. The HFA assumes that the angular momentum of the odd particle is frozen aligned with one of principal axis of the nucleus and can be considered as a number j. In this way, the wobbling energy can be approximated as [2]

$$\hbar\omega_w = \frac{j}{\mathcal{J}_3}\left[\left(1+\frac{J}{j}\left(\frac{\mathcal{J}_3}{\mathcal{J}_1}-1\right)\right)\left(1+\frac{J}{j}\left(\frac{\mathcal{J}_3}{\mathcal{J}_2}-1\right)\right)\right]^{1/2}. \tag{2}$$

By adjusting the value of j, the impact of the magnitude of angular momentum on wobbling energy can be reflected, as shown in Fig. 7. We fix j on the s axis (low spin) and m axis (high spin) and calculate the wobbling energy using Eq. (2). It can be seen that the larger j corresponds to the larger wobbling energy, which applies to both low and high spin regions. This is helpful for qualitatively understanding the influence of quadrupole deformation parameters on wobbling energy in different spin regions. According to Fig. 4, we observe that at the beginning of the rotation of the TW region, the s component with larger β is larger than that with smaller β. In the end of the spin region of the LW region, the m axis component with smaller β is larger. This explains why the nucleus with smaller β has smaller wobbling energy in the low spin region, whereas has larger wobbling energy in the high spin region.

E. Compare with experimental data

In order to investigate the behavior of wobbling motion in realistic nuclei under varying nuclear deformations, we

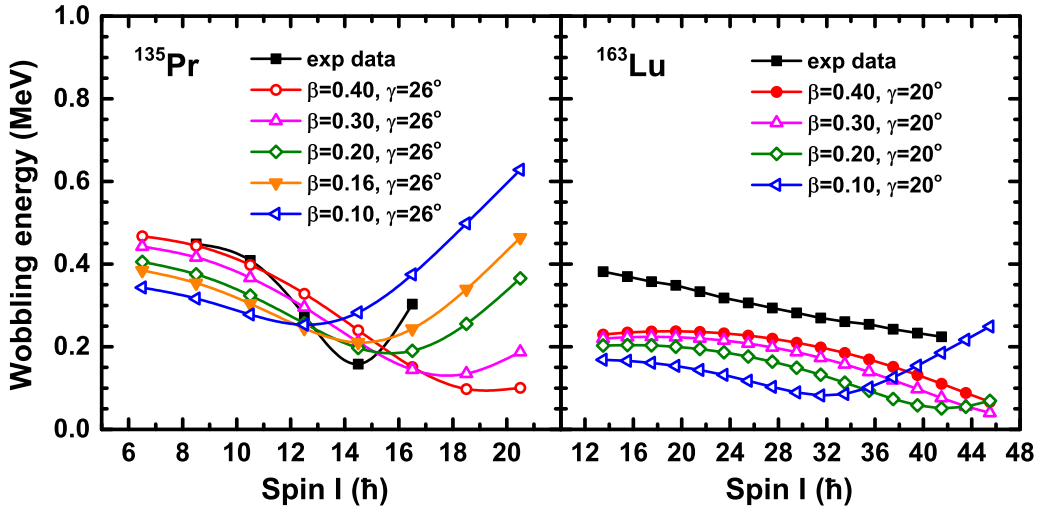

FIG. 8. Calculated wobbling energies as functions of spin I by the PRM with different deformation parameter β in comparison with the experimental data for the ^{135}Pr (left) and ^{163}Lu (right).

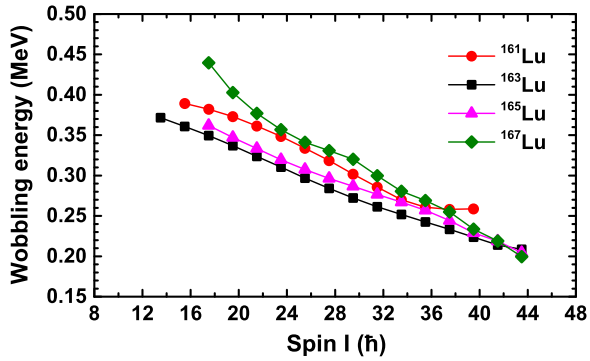

FIG. 9. Experimental wobbling energies as functions of spin I for ^{161,163,165,167}Lu. The data are extracted from Refs. [4,6–8].

conducted a detailed study focusing on two distinct cases: the low deformation nucleus ^{135}Pr ($\beta \approx 0.16$) [11] and the strongly deformed nucleus ^{163}Lu ($\beta \approx 0.40$) [4]. Our analysis, depicted in Fig. 8, presents the calculated wobbling energies as functions of spin I using the PRM with different deformation parameters β, alongside experimental data for ^{135}Pr and ^{163}Lu. In our calculations, we utilized input configuration, moments of inertia, and triaxial deformation parameters from Ref. [2]: $\pi(1h_{11/2})^1$ configuration with $\mathcal{J}_{m,s,l} = 21$, 13, 4 $\hbar^2$/MeV and $\gamma = 26^\circ$ for ^{135}Pr, and $\pi(1i_{13/2})^1$ configuration with $\mathcal{J}_{m,s,l} = 64$, 56, 13 $\hbar^2$/MeV and $\gamma = 20^\circ$ for ^{163}Lu.

For ^{135}Pr, the experimental wobbling frequencies exhibit a decreasing trend with spin for $I \leqslant 14.5\hbar$, indicative of transverse wobbling motion [11]. Beyond $I > 14.5\hbar$, the wobbling frequency shows an increasing pattern, suggesting a transition from transverse to longitudinal wobbling mode [11], with the critical spin value for this transition identified as $I = 14.5\hbar$. This instability is expected from the changes in the effective moments of inertia for example by using the HFA approximation or by the microscopic cranked shell model plus random phase approximation calculations [28,30,32]. Maintaining a constant γ in the PRM calculations, we observed that smaller β values correspond to lower critical spin values. Specifically, a $\beta = 0.16$ was found to align well with experimental data for ^{135}Pr.

In the case of ^{163}Lu, experimental data displayed a gradual decrease in wobbling energy, indicating a stable TW mode across the spin region. The instable TW observed at low spin in ^{135}Pr is not observed in ^{163}Lu. The decreasing trend in wobbling energy was successfully reproduced with $\beta = 0.40$ and 0.30. The initial increase in theoretical results was attributed to the moment of inertia $\mathcal{J}_m$ being only slightly greater than $\mathcal{J}_s$, consistent with previous findings [2], underscoring the sensitivity of the wobbling mode to the axis ratio of moments of inertia [47]. Similar to ^{135}Pr, smaller β values in ^{163}Lu led to lower critical spin values. Notably, PRM calculations with $\beta = 0.20$ and 0.10 yield critical spin values that are too small for ^{163}Lu, highlighting the significant impact of the β deformation parameter on the wobbling motion within the nucleus.

Furthermore, the study of wobbling motion in an isotope or isotone is valuable to check the deformation dependence of the wobbling motion. For this purpose, we summarize the wobbling energies of the $n = 1$ wobbling bands observed in ^{161,163,165,167}Lu [4,6–8] in Fig. 9. As illustrated in the figure, the wobbling energy decreases with increasing spin, indicating that they are all TW. In the cranking calculations utilizing the ultimate cranker (UC) method, based on a modified harmonic oscillator potential, the deformation parameters of these isotopes were predicted as follows: ^{161}Lu ($\beta = 0.40, \gamma = 20^\circ$) [6], ^{163}Lu ($\beta = 0.40, \gamma = 20^\circ$) [4], ^{165}Lu ($\beta = 0.40, \gamma = 20^\circ$) [7], and ^{167}Lu ($\beta = 0.43, \gamma = 19^\circ$) [8]. We further performed the constrained covariant density functional theory (CDFT) [55,56] calculations with effective interaction PC-PK1 [57] for these four isotopes based on the $i_{13/2}$ configuration. The deformation parameters are predicted as follows: ^{161}Lu ($\beta = 0.52, \gamma = 12^\circ$), ^{163}Lu ($\beta = 0.48, \gamma = 11^\circ$), ^{165}Lu ($\beta = 0.48, \gamma = 10^\circ$), and ^{167}Lu ($\beta = 0.64, \gamma = 13^\circ$). It is observed that the CDFT predicts relatively larger β but smaller γ values than the UC method. Nevertheless, in both calculations, the β deformation values are relatively large. Consequently, the wobbling motion in these strongly deformed nuclei is anticipated to persist over a broader range of spin values compared to those in normally deformed nuclei, aligning with prior findings.

Upon closer examination, however, it is noted that the magnitudes of wobbling energy differ among these four nuclei. Specifically, within the spin region $I \leqslant 35.5\hbar$, the ordering of wobbling energy from smallest to largest is observed to be ^{163}Lu, ^{165}Lu, ^{161}Lu, and ^{167}Lu. This observed ordering does not fully align with the anticipated trend based solely on predicted β deformation in the UC results, where larger β values are expected to correspond to larger wobbling energy. On the contrary, the CDFT calculations corroborate this trend with respect to the β deformation parameters. However, notably, the CDFT predictions yield quite small γ values, even less than 15°. Indeed, other factors such as moments of inertia along the three principal axes in realistic nuclei are likely to influence the dynamics of the wobbling motion. For example, in the microscopic cranked shell model plus random phase approximation calculations [28,30,32], the moments of inertia varies with the rotation. Correspondingly, the wobbling energy trend can also change. However, in the present work, the moments of inertia are fixed and show somewhat limitations in the descriptions for the realistic nuclei. This suggests that a more nuanced understanding of the underlying physics is necessary.

IV. SUMMARY

In summary, the PRM has been used to investigate the influence of deformation parameters β and γ on the wobbling motion. The valence nucleon $h_{11/2}$ and $i_{13/2}$ combined with a triaxial core are considered as examples. The influences of deformation on the wobbling mode are studied through the analysis of wobbling energy, electromagnetic transition probabilities, and angular momentum components.

Within the investigated range of deformation, larger quadrupole deformation β and smaller triaxial deformation γ are more likely to form TW. A smaller β corresponds to a smaller transverse wobbling energy, while a larger

longitudinal wobbling energy. These behaviors can be well explained by the HFA approximation method. In comparison to γ, LW exhibit higher sensitivity to β. The $B(E2)_{\rm out}/B(E2)_{\rm in}$ ratios of $h_{11/2}$ and $i_{13/2}$ configurations shows great similarity with different β, while the variation rate of $B(M1)_{\rm out}/B(E2)_{\rm in}$ is more significant at different β.

The impact on the angular momentum mainly stems from the competition between the s and m axes. With the same β value, increasing the triaxial deformation parameter γ leads to a larger initial angular momentum in the s axis and a smaller angular momentum in the m axis for the valence nucleon. As spin increases, the angular momentum decreases in the s axis and increases in the m axis. The finding that the TW under the large β can maintain a wide range can be understood by the analysis of the P_n plot and $h_{11/2}$ shell single-particle energy levels. The behavior of wobbling motion in nuclei under varying nuclear deformations is tested on two distinct cases: the low deformation nucleus ^{135}Pr and the strongly deformed nucleus ^{163}Lu.

Finally, it should be pointed out that the current work fixed the moments of inertia $\mathcal{J}_0$ as a constant. This is not very realistic as the moment of inertia $\mathcal{J}_0$ is in fact in direct proportion to β^2 [1,58]. In addition, the wobbling mode is quite sensitive to the adopted axis ratio of the moments of inertia [47,59]. In our model study, we use irrotational flow type moment of inertia. In realistic nuclei, this kind of ratio can be modified, e.g., as in the cases of ^{135}Pr and ^{163}Lu as we have shown. Further considering this fact is needed. One of the ways is adopting the RPA method [26–37], which can predict moments of inertia microscopically. The other way is adopting the mean-field theory, e.g., covariant density functional theory [56], to provide microscopic moments of inertia for PRM calculations. Moreover, very high spin energy levels cannot be solely explained by assuming a rigid triaxial core and one particle. Several other effects, such as multiparticle modes, can significantly influence the energy spectra and will be considered in future research.

ACKNOWLEDGMENT

This work was supported by the National Natural Science Foundation of China under Grant No. 12205103.

[1] A. Bohr and B. R. Mottelson, *Nuclear Structure*, Vol. II (Benjamin, New York, 1975).
[2] S. Frauendorf and F. Dönau, Phys. Rev. C **89**, 014322 (2014).
[3] Q. B. Chen and S. Frauendorf, Eur. Phys. J. A **58**, 75 (2022).
[4] S. W. Ødegård, G. B. Hagemann, D. R. Jensen, M. Bergstrom, B. Herskind, G. Sletten, S. Törmänen, J. N. Wilson, P. O. Tjøm, I. Hamamoto, K. Spohr, H. Hubel, A. Gorgen, G. Schonwasser, A. Bracco, S. Leoni, A. Maj, C. M. Petrache, P. Bednarczyk, and D. Curien, Phys. Rev. Lett. **86**, 5866 (2001).
[5] D. R. Jensen, G. B. Hagemann, I. Hamamoto, S. W. Odegard, B. Herskind, G. Sletten, J. N. Wilson, K. Spohr, H. Hubel, P. Bringel, A. Neusser, G. Schonwasser, A. K. Singh, W. C. Ma, H. Amro, A. Bracco, S. Leoni, G. Benzoni, A. Maj, C. M. Petrache, G. LoBianco, P. Bednarczyk, and D. Curien, Phys. Rev. Lett. **89**, 142503 (2002).
[6] P. Bringel, G. B. Hagemann, H. Hübel, A. Al-Khatib, P. Bednarczyk, A. Bürger, D. Curien, G. Gangopadhyay, B. Herskind, D. R. Jensen *et al.*, Eur. Phys. J. A **24**, 167 (2005).
[7] G. Schönwaßer, H. Hübel, G. B. Hagemann, P. Bednarczyk, G. Benzoni, A. Bracco, P. Bringel, R. Chapman, D. Curien, J. Domscheit *et al.*, Phys. Lett. B **552**, 9 (2003).
[8] H. Amro, W. C. Ma, G. B. Hagemann, R. M. Diamond, J. Domscheit, P. Fallon, A. Görgen, B. Herskind, H. Hübel, D. R. Jensen *et al.*, Phys. Lett. B **553**, 197 (2003).
[9] D. J. Hartley, R. V. F. Janssens, L. L. Riedinger, M. A. Riley, A. Aguilar, M. P. Carpenter, C. J. Chiara, P. Chowdhury, I. G. Darby, U. Garg, Q. A. Ijaz, F. G. Kondev, S. Lakshmi, T. Lauritsen, A. Ludington, W. C. Ma, E. A. McCutchan, S. Mukhopadhyay, R. Pifer, E. P. Seyfried, I. Stefanescu, S. K. Tandel, U. Tandel, J. R. Vanhoy, X. Wang, S. Zhu, I. Hamamoto, and S. Frauendorf, Phys. Rev. C **80**, 041304(R) (2009).
[10] A. Mukherjee, S. Bhattacharya, T. Trivedi, S. Tiwari, R. P. Singh, S. Muralithar, Yashraj, K. Katre, R. Kumar, R. Palit, S. Chakraborty, S. Jehangir, N. Nazir, S. P. Rouoof, G. H. Bhat, J. A. Sheikh, N. Rather, R. Raut, S. S. Ghugre, S. Ali, S. Rajbanshi, S. Nag, S. S. Tiwary, A. Sharma, S. Kumar, S. Yadav, and A. K. Jain, Phys. Rev. C **107**, 054310 (2023).
[11] J. T. Matta, U. Garg, W. Li, S. Frauendorf, A. D. Ayangeakaa, D. Patel, K. W. Schlax, R. Palit, S. Saha, J. Sethi *et al.*, Phys. Rev. Lett. **114**, 082501 (2015).
[12] N. Sensharma, U. Garg, S. Zhu, A. D. Ayangeakaa, S. Frauendorf, W. Li, G. H. Bhat, J. A. Sheikh, M. P. Carpenter, Q. B. Chen *et al.*, Phys. Lett. B **792**, 170 (2019).
[13] S. Biswas, R. Palit, S. Frauendorf, U. Garg, W. Li, G. H. Bhat, J. A. Sheikh, J. Sethi, S. Saha, P. Singh *et al.*, Eur. Phys. J. A **55**, 159 (2019).
[14] C. M. Petrache, P. M. Walker, S. Guo, Q. B. Chen, S. Frauendorf, Y. X. Liu, R. A. Wyss, D. Mengoni, Y. H. Qiang, A. Astier *et al.*, Phys. Lett. B **795**, 241 (2019).
[15] Q. B. Chen, S. Frauendorf, and C. M. Petrache, Phys. Rev. C **100**, 061301(R) (2019).
[16] Y. K. Wang, F. Q. Chen, and P. W. Zhao, Phys. Lett. B **802**, 135246 (2020).
[17] S. Chakraborty, H. P. Sharma, S. S. Tiwary, C. Majumder, A. K. Gupta, P. Banerjee, S. Ganguly, S. Rai, S. Kumar, A. Kumar *et al.*, Phys. Lett. B **811**, 135854 (2020).
[18] K. R. Devi, S. Kumar, N. Kumar, F. S. Babra, M. S. Laskar, S. Biswas, S. Saha, P. Singh, S. Samanta, S. Das *et al.*, Phys. Lett. B **823**, 136756 (2021).
[19] F.-Q. Chen and C. M. Petrache, Phys. Rev. C **103**, 064319 (2021).
[20] B. F. Lv, C. M. Petrache, R. Budaca, A. Astier, K. K. Zheng, P. Greenlees, H. Badran, T. Calverley, D. M. Cox, T. Grahn *et al.*, Phys. Rev. C **105**, 034302 (2022).
[21] N. Sensharma, U. Garg, Q. B. Chen, S. Frauendorf, D. P. Burdette, J. L. Cozzi, K. B. Howard, S. Zhu, M. P. Carpenter, P. Copp *et al.*, Phys. Rev. Lett. **124**, 052501 (2020).
[22] S. Nandi, G. Mukherjee, Q. B. Chen, S. Frauendorf, R. Banik, S. Bhattacharya, S. Dar, S. Bhattacharyya,

C. Bhattacharya, S. Chatterjee *et al.*, Phys. Rev. Lett. **125**, 132501 (2020).
[23] J. Timár, Q. B. Chen, B. Kruzsicz, D. Sohler, I. Kuti, S. Q. Zhang, J. Meng, P. Joshi, R. Wadsworth, K. Starosta *et al.*, Phys. Rev. Lett. **122**, 062501 (2019).
[24] H. M. Dai, Q. B. Chen, and X.-R. Zhou, Phys. Rev. C **108**, 054306 (2023).
[25] L. Hu, J. Peng, and Q. B. Chen, Phys. Rev. C **104**, 064325 (2021).
[26] E. R. Marshalek, Nucl. Phys. A **331**, 429 (1979).
[27] Y. R. Shimizu and M. Matsuzaki, Nucl. Phys. A **588**, 559 (1995).
[28] M. Matsuzaki, Y. R. Shimizu, and K. Matsuyanagi, Phys. Rev. C **65**, 041303(R) (2002).
[29] M. Matsuzaki, Y. R. Shimizu, and K. Matsuyanagi, Eur. Phys. J. A **20**, 189 (2003).
[30] M. Matsuzaki, Y. R. Shimizu, and K. Matsuyanagi, Phys. Rev. C **69**, 034325 (2004).
[31] M. Matsuzaki and S. I. Ohtsubo, Phys. Rev. C **69**, 064317 (2004).
[32] Y. R. Shimizu, M. Matsuzaki, and K. Matsuyanagi, arXiv:nucl-th/0404063.
[33] Y. R. Shimizu, M. Matsuzaki, and K. Matsuyanagi, Phys. Rev. C **72**, 014306 (2005).
[34] D. Almehed, R. G. Nazmitdinov, and F. Doenau, Phys. Scr. **T125**, 139 (2006).
[35] Y. R. Shimizu, T. Shoji, and M. Matsuzaki, Phys. Rev. C **77**, 024319 (2008).
[36] T. Shoji and Y. R. Shimizu, Prog. Theor. Phys. **121**, 319 (2009).
[37] S. Frauendorf and F. Dönau, Phys. Rev. C **92**, 064306 (2015).
[38] Q. B. Chen, S. Q. Zhang, P. W. Zhao, and J. Meng, Phys. Rev. C **90**, 044306 (2014).
[39] Q. B. Chen, S. Q. Zhang, and J. Meng, Phys. Rev. C **94**, 054308 (2016).
[40] Q. B. Chen and S. Frauendorf, Phys. Rev. C **109**, 044304 (2024).
[41] M. Shimada, Y. Fujioka, S. Tagami, and Y. R. Shimizu, Phys. Rev. C **97**, 024318 (2018).
[42] I. Hamamoto, Phys. Rev. C **65**, 044305 (2002).
[43] I. Hamamoto and G. B. Hagemann, Phys. Rev. C **67**, 014319 (2003).
[44] E. Streck, Q. B. Chen, N. Kaiser, and Ulf-G. Meißner, Phys. Rev. C **98**, 044314 (2018).
[45] Q. B. Chen, S. Frauendorf, N. Kaiser, U.-G. Meißner, and J. Meng, Phys. Lett. B **807**, 135596 (2020).
[46] C. Broocks, Q. B. Chen, N. Kaiser, and U.-G. Meißner, Eur. Phys. J. A **57**, 161 (2021).
[47] H. Zhang, B. Qi, X. D. Wang, H. Jia, and S. Y. Wang, Phys. Rev. C **105**, 034339 (2022).
[48] S. H. Li, H. M. Dai, Q. B. Chen, and X.-R. Zhou, Chin. Phys. C **48**, 034102 (2024).
[49] K. Tanabe and K. Sugawara-Tanabe, Phys. Rev. C **95**, 064315 (2017).
[50] R. Budaca, Phys. Rev. C **97**, 024302 (2018).
[51] E. A. Lawrie, O. Shirinda, and C. M. Petrache, Phys. Rev. C **101**, 034306 (2020).
[52] R. Budaca, Phys. Rev. C **103**, 044312 (2021).
[53] R. Budaca and C. M. Petrache, Phys. Rev. C **106**, 014313 (2022).
[54] D. J. Hartley, R. V. F. Janssens, L. L. Riedinger, M. A. Riley, X. Wang, A. Aguilar, M. P. Carpenter, C. J. Chiara, P. Chowdhury, I. G. Darby *et al.*, Phys. Rev. C **83**, 064307 (2011).
[55] J. Meng, J. Peng, S. Q. Zhang, and S.-G. Zhou, Phys. Rev. C **73**, 037303 (2006).
[56] *Relativistic Density Functional for Nuclear Structure*, Vol. 10 of International Review of Nuclear Physics, edited by J. Meng (World Scientific, Singapore, 2016).
[57] P. W. Zhao, Z. P. Li, J. M. Yao, and J. Meng, Phys. Rev. C **82**, 054319 (2010).
[58] P. Ring and P. Schuck, *The Nuclear Many Body Problem* (Springer Verlag, Berlin, 1980).
[59] S. Frauendorf, Phys. Rev. C **97**, 069801 (2018).